Sustainable and scalable *in-situ* synthesis of hydrochar-wrapped Ti_3AlC_2-derived nanofibers as adsorbents to remove heavy metals

Xinsheng Dong[1], Yaquan Wang[1], Mingmin Jia[1], Zhaoyang Niu[1], Junmeng Cai[2], Xuebin Ke[3], Xingguang Zhang[1]* and Jianfeng Yao[1]*

Address:

1. College of Chemical Engineering, Jiangsu Key Lab for the Chemistry & Utilization of Agricultural and Forest Biomass, Nanjing Forestry University, Nanjing, Jiangsu 210037, P. R. Email: x.g.zhang@njfu.edu.cn Email: jfyao@njfu.edu.cn

2. Biomass Energy Engineering Research Center, School of Agriculture and Biology, Shanghai Jiao Tong University, 800 Dongchuan Road, Shanghai 200240, P.R. China

3. School of Engineering and Computer Science, University of Hull, HU6 7RX, UK.

Abstract:

To ensure a sustainable future, it is imperative to efficiently utilize abundant biomass to produce such as platform chemicals, transport fuels, and other raw materials; hydrochar is one of the promising candidates derived by hydrothermal carbonization of biomass in compressed water. They synthesis of "hydrochar-wrapped Ti_3AlC_2-derived nanofibers (HCTNFs)" was successfully achieved by the facile one-pot hydrothermal reaction using glucose as the hydrochar precursor. Meanwhile, cellulose and sawdust as raw materials were also investigated. HCTNFs were characterized by: XRD, N_2 adsorption-desorption isotherms, SEM, TEM, FT-IR, and EDS to investigate their crystal structures, textural properties, morphologies, surface species and elemental compositions. In the adsorption test to remove Cd(II) and Cu(II) in aqueous solution, HCTNFs outperformed pure nanofibers derived from Ti_3AlC_2, Hydrothermal carbon derived from glucose and commercial activated carbon; finally the regeneration and sorption kinetics were also studied.

Key words: Hydrochar, Ti_3AlC_2, adsorption; heavy metals.

Highlights

1. Hydrochar-wrapped nanofibers (HCTNFs) derived from Ti_3AlC_2 MAX phases were successfully prepared using glucose as the hydrochar precursor.
2. HCTNFs exhibited much higher adsorptive performances as to Cd(II) and Cu(II) compared with pure nanofibers derived from Ti_3AlC_2, hydrothermal carbon derived from glucose, and commercial activated carbon.
3. Using cellulose or pinewood sawdust as hydrochar precursors, adsorption capacities were also enhanced, offering a sustainable and scalable process to prepare high-performance adsorbents
4. Adsorbents are prepared by fluoride-free hydrothermal reaction and fibrerous materials are easily recyclable after use.

Introduction

Rapid developments of industrialization and burgeoning increase in population have depleted nonrenewable resources and polluted natural environments. It is promising to ensure a sustainable future via efficient exploitation of abundant biomass to produce such as platform chemicals, transport fuels, and other raw materials.[1, 2] Hydrochar is one of the promising candidates derived from hydrothermal carbonization of biomass in compressed hot water (130-250^{o}C). Compared with slow-pyrolysis of biomass at high temperatures (300-650^{o}C) to yield biochar, the hydrothermal carbonization process possesses advantages of cost-efficiency and convenience in direct utilization of wet feedstock without pre-drying requirement.[3] The hydrochar produced differs significantly from biochar in physiochemical properties that determine their potential applications in such as agriculture, energy production, environmental protection, catalysis and adsorption.[4, 5]

The presence of heavy metals in water resources poses a detrimental effect on human beings and aquatic lives.[6, 7] For instance, copper ions once ingested excessively in the human diet may cause itching, dermatitis, vomiting, cramps, convulsions, and even death;[8] Cadmium (Cd) has been classified as a human carcinogen and teratogen impacting lungs, kidneys, liver and reproductive organs.[9] The remediation of polluted water remains a urgent issue particularly in underdeveloped countries, and measures of adsorption,[10] chemical deposition,[11] electrodialysis,[12] ion exchange,[13] solvent extraction,[14] distillation,[15] ultra filtration,[16] and reverse osmosis[17] have been taken to remove heavy metals from wasted water. Among these methods, adsorption technology is inexpensive, easily scalable, and relatively environmental-friendly, and thus the activated carbon-based adsorbents are quite popular; however, activated carbon has limited adsorption capacity for heavy metal ions, owing to insufficient adsorptive sites.[18] In this regard, the aforementioned eco-friendly hydrochar is a promising substitute for their competency to capture heavy metals (e.g. Hg^{2+}, Cu^{2+}) in aqueous solution.[19, 20] Studies have demonstrated that hydrocar possesses abundant surface functional groups (e.g., COOH, OH, CO) to ensure remarkably enhanced adsorption capacity for heavy metals by electrostatic attraction, ion exchange, and surface complexation.[21, 22]

Recently, composite adsorbents of attapulgite clay@carbon heterogeneous structures are prepared by a one-pot hydrothermal process, and outperform carbon-based materials to remove heavy metals of Cr(VI) and Pb(II).[23]

These studies inspire us to envisage that the Ti_3AlC_2 MAX phases should be an excellent candidate to combine with hydrochar because they have typical layered ternary metal carbides, nitrides, or carbonitrides[24] and can achieve functional surface species after treatment with exfoliation. Reports have focused on their electrical, thermal and mechanical properties[25] and structural evolution into MXenes (e.g. Ti_3C_2, Ti_2C) and other nanomaterials[26] or composites.[27] However, few studies systematically investigate its transformation to nanofiberous materials. This work develops a scalable *in-situ* synthetic method to prepare "hydrochar-wrapped Ti_3AlC_2-derived nanofibers" (denoted as HCTNFs), utilizing glucose, cellulose or pinewood sawdust as the hydrochar precursors. To our best knowledge, there are no reports on the *in-situ* combination of TNFs with hydrochar as adsorbents for removal of heavy metals. The experimental results reveal that the bonded interfacial materials formed between hydrochar and nanofibers offers an intrinsically strong and stable structure. In the adsorption of Cu(II) and Cd(II), these new adsorbents outperform their counterparts of hydrothermal carbon derived from glucose, activated carbon and pure nanofibers owing to the fully exposed surface oxygenated functionalities. These findings are encouraging and should spark more studies on utilizing biomass-based materials for other applications in such as catalysis, materials design and energy storage.[2, 4, 28]

Experimental section

Raw Materials

The following chemicals were purchased: Ti_3AlC_2 (~98% purity), NaOH (96%, Xilong Scientific Co., Ltd., China), $Cd(CH_3COO)_2{\cdot}2H_2O$ (chemical reagents, Sinopharm Chemical Reagent Co. Ltd., China), $CuSO_4{\cdot}5H_2O$ (99%, Shanghai Xinbao Fine Chemical Factory, China), $C_6H_{12}O_6{\cdot}H_2O$ (analytical reagents, Sinopharm Chemical Reagent Co.,Ltd., China), Microcrystalline cellulose (analytical reagents, Tianjin Guangfu Fine Chemical Research Institute, China), Sawdust (Liuan, Anhui, China).

Optimization of the synthesis of "Ti_3AlC_2-derived nanofibers" (TNFs)

The transformation of Ti_3AlC_2 MAX phases was derived from the method reported in our previous study.[29] Typically, 3 g of the Ti_3AlC_2 particles were mixed with 40 mL of NaOH aqueous solution (10 mol/L) under stirring for 24 h at room temperature. After stirring, the suspension was transferred into a 100-mL autoclave with a PTFE container inside. The autoclave was maintained at temperature of 180°C for 48h in an oven under static conditions. Following hydrothermal treatment and cooling down to room temperature naturally, the solid products were recovered by filtration, washed with deionized water to remove excessive NaOH, until the pH = 7-9. Then the samples were dried at 60°C overnight without further treatment. Additionally, to optimize synthetic conditions, the concentration of NaOH aqueous solution, hydrothermal temperatures, and reaction time were systematically optimized. Detailed experimental information and the associated characterization results were provided in the **Section 1**, **ESI**.

Synthesis of "hydrochar-wrapped Ti_3AlC_2-derived nanofibers" (HCTNFs)

The hydrothermal conditions to synthesize HCTNFs were performed under the aforementioned optimized experimental conditions, using three different precursors: glucose, cellulose, and pinewood sawdust. The Glu@TNFs was synthesized as the following procedures: 1 g of Ti_3AlC_2 MAX powder (200 mesh) was mixed with 15 mL of 10 mol L^{-1} NaOH solution. The suspension was continuously stirred for 3h at ambient conditions. 1, 2, or 4 g of glucose was mixed with the solution respectively and stirred for 1h. The solution was subsequently transferred into a 100-mL autoclave with a PTFE container inside. The autoclave was maintained at 180°C for 48 h under static conditions. The precipitate was recovered and washed with distilled water to remove excessive NaOH, until the pH ranged from 7 to 9. Finally, the precipitate was washed with ethanol and then the obtained product was dried at 80 °C for 12 h. The samples prepared with different weight ratios of glucose/Ti_3AlC_2, and the products were denoted as Glu@TNFs-1, Glu@TNFs-2, Glu@TNFs-3. For comparison, 1 g of glucose was also hydrothermally treated under the same conditions, and the final product was denoted as hydrothermal carbon. The Cel@TNFs was synthesized by the same procedure as Glu@TNFs, except for the use of cellulose instead

of glucose. 0.9, 1.8, or 3.6 g of cellulose was mixed with the solution and stirred for 1h. The samples prepared with different weight ratios of cellulose/Ti_3AlC_2 were denoted as Cel@TNFs-1, Cel@TNFs-2, Cel@TNFs-3. The Saw@TNFs was synthesized by the same procedure as Glu@TNFs, except using sawdust instead of glucose. 2, 4, or 8 g of sawdust was mixed with the solution and stirred for 1h. The samples prepared with different weight ratios of sawdust/Ti_3AlC_2 were denoted as Saw@TNFs-1, Saw@TNFs-2, Saw@TNFs-3. (Note: the amount of cellulose or sawdust added was according to the estimation that 1 g of glucose can be produced by hydrolyzing 0.9 g of cellulose or 2 g sawdust.[30, 31]

Characterizations

The crystal phases of samples were analyzed by X-ray diffraction (XRD) using Rigaku Smartlab with Cu Kα radiation (λ = 0.1542 nm) at a scan rate of 5°/min from 5 to 80 (2θ) at a voltage of 40 kV. Fourier transform infrared spectra (FTIR) was used to detect the surface functional groups by a FTIR spectrophotometer (Thermo Electron Nicolet-360, USA) using the KBr wafer technique 400-4000 cm^{-1}. The morphology of the samples was examined by Field-emission scanning electron microscopy (FESEM) utilizing a JSM-7600F (JEOL Ltd., Japan) with an operating voltage of 30 kV. Transmission electron microscopy (TEM) images were obtained by a JEOL JEM-2100 instrument at the accelerating voltage of 200 kV. The compositions of the samples were analyzed by energy-dispersive X-ray spectroscopy (EDX) attached to the FESEM instrument. Five random spots have been performed to calculate the elemental composition. Zeta potentials were measured by the ZETASIZER Nano-ZS from Malvern Instruments with the liquid concentration of 0.75 mg/mL at initial pH value (~6). Nitrogen (N_2) adsorption-desorption analysis was conducted using the Micromeritics ASAP 2020 at 77 K. The specific surface areas were measured by the Brunauer-Emmett-Teller (BET) method. The concentration of Cd(II) and Cu(II) were determined by an atomic absorption spectrometer (PinAAcle 900F, American PerkinElmer).

Adsorptive capacity test

A stock solution of 100 mg L^{-1} Cd(II) or Cu(II) was prepared using $Cd(CH_3COO)_2 \cdot 2H_2O$ or $CuSO_4 \cdot 5H_2O$ in distilled water. The adsorption capacity of different composites was calculated according to the equation:

$$q_e=(C_0-C_e)V/m \quad (1)$$

Where q_e (mg g^{-1}) was the adsorption capacity at equilibrium, C_0 (mg L^{-1}) was the initial concentration of Cu(II) or Cd(II) and C_e (mg L^{-1}) was the equilibrium concentration of Cu(II) or Cd(II); V (mL) and m (mg) represented the volume of the solution and the mass of the adsorbent, respectively.

The adsorption kinetics experiments were performed to evaluate the adsorption rates of Cd(II) or Cu(II) on the representative adsorbent of Glu@TNFs-3, Cel@TNFs-3, and Saw@TNFs-3. The initial concentration of Cd(II) or Cu(II) was 100 mg L^{-1}. Typically, 15 mg of sample was added in 15 ml of the tested solution, and the suspension was stirred at room temperature for 24h to reach the equilibrium; then the concentration of metal ions was determined by an atomic absorption spectrometer. In order to further determine the contact time required to reach the equilibrium and to understand the rate of the sorption process, pseudo-first-order and pseudo-second-order were exploited to simulate the experimental data. The pseudo-first-order kinetic model and pseudo-second-order kinetic models are presented as follows:

$$\ln(q_e - q_t) = \ln q_e - k_1 t \quad (2)$$

$$t/q_t = 1/(k_2 q_e^2) + t/q_e \quad (3)$$

Where q_e and q_t are the adsorption capacities (mg g^{-1}) at equilibrium time and at the time of t (min), respectively; k_1 (min^{-1}) and k_2 (g mg^{-1} min^{-1}) represent the rate constant of the pseudo-first-order and pseudo-second-order models, respectively.

Results and discussions

Characterization of "hydrochar-wrapped Ti_3AlC_2-derived nanofibers" (HCTNFs)

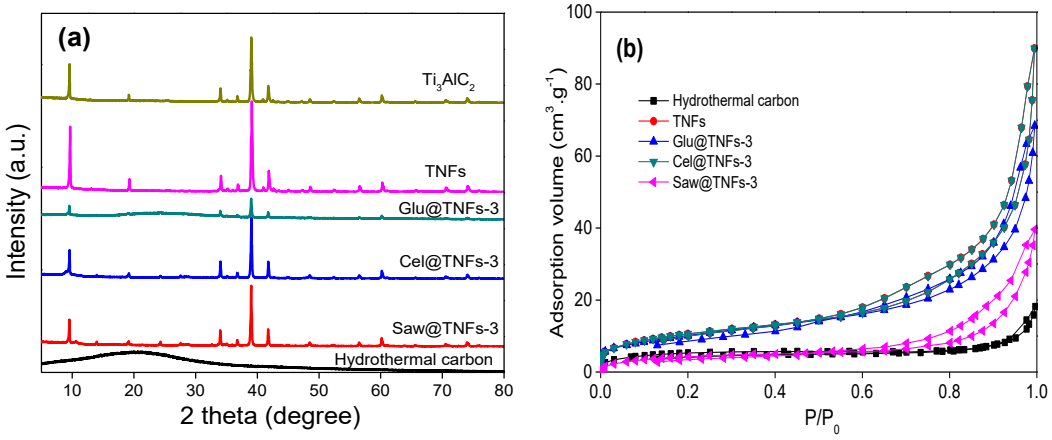

Fig. 1 XRD patterns **(a)** and N_2 adsorption–desorption isotherms (**b)** of the parent Ti_2AlC_3, TNFs, Glu@TNFs-3, Cel@TNFs-3, Saw@TNFs-3, and Hydrothermal carbon. Synthetic conditions: 10 mol/L NaOH aqueous solution, 180ºC, 48h

The crystallographic structures of the pristine Ti_3AlC_2, TNFs, Glu@TNFs-3, Cel@TNFs-3, Saw@TNFs-3, and Hydrothermal carbon (derived from glucose) were characterized by XRD. As shown in **Fig. 1a**, the diffraction peaks at 9.5°, 19.1°, 36.7°, 38.1°, 39°, 41.7°, 48.4° and 60.1°are assigned to the crystal facets of (002), (004), (101), (103), (008), (105), (107) and (110), corresponding to the typi1cal crystal phases of Ti_3AlC_2 (JCPDS no. 52-0875).[32, 33] After hydrothermal treatment of Ti_3AlC_2 by concentrated NaOH solution, Ti_3AlC_2 was transformed into nanosheets, nanofibers or bulk particles, essentially depending upon the hydrothermal conditions (e.g. concentrations of NaOH solution, hydrothermal temperatures, and reaction time; more information can be found in **Section 1**, **ESI**. The crystal structure evolution, the morphological transformation, and the possible mechanism were also provided.).[34] In this work, the nanofibers were prepared under the optimized hydrothermal conditions (10 mol/L NaOH solution, 180ºC and 48h, and the final products were denoted as TNFs), they preserved the primary characteristic peaks of Ti_3AlC_2, and also showed newly-appeared peaks at the 2θ of 10.3º, 25.0º and 29.7º. In contrast, the Hydrothermal carbon derived from glucose exhibited no sharp peaks but a broad peak at 2θ angles of 10-30º, which were attributed to the (002) plane of amorphous carbon, revealing that glucose had been carbonized.[35, 36] The Glu@TNFs-3 exhibited sharp peaks of TNFs with

much lower intensities and broad peaks of amorphous carbon, demonstrating a composite structure of them. For Cel@TNFs-3 and Saw@TNFs-3, the characteristic peaks of TNFs was lower compared with those of pure TNFs, and the broad peaks of amorphous carbon were not as identifiable as those of Glu@TNFs-1, probably because the hydrochar formed was heterogeneously coated on the surface of TNFs (all XRD patterns of Glu@TNFs, Cel@TNFs, and Saw@TNFs were provided in **Section 2**, **ESI**).

The N_2 adsorption-desorption isotherms of Hydrothermal carbon, TNFs, Glu@TNFs-3, Cel@TNFs-3 and Saw@TNFs-3 are shown in **Fig. 1 (Right)**. The HCTNFs exhibit a typical type IV isotherm with a hysteresis loop attributable to the presence of the mesoporous structure in the HCTNFs;[37] In addition, the hysteresis loops formed between 0.8-1.0 (P/P_0) are mainly due to the formation of inter-particle avoids. According to BET measurements, the specific surface areas are obtained as the following: Hydrothermal carbon (19.4 $m^2\ g^{-1}$), TNFs (1.0 $m^2\ g^{-1}$), Glu@TNFs-3 (37.0 $m^2\ g^{-1}$), Cel@TNFs-3 (38.9 $m^2\ g^{-1}$), and Saw@TNFs-3 (16.2 $m^2\ g^{-1}$) (The BET surface areas of all Glu@TNFs, Cel@TNFs and Saw@TNFs can be found in the **Section 3**, **ESI**, and the N_2 adsorption-desorption isotherms of these aforementioned samples were given in **Section 4**, **ESI**). The specific surface areas of HCTNFs nanofibers were much higher than that of pristine Ti_3AlC_2 powder (1.2 $m^2\ g^{-1}$) and the urchin-like rutile titania carbon composites of e-TACFs and e-TACSs (16.4 $m^2\ g^{-1}$ and 1.6 $m^2\ g^{-1}$).[34, 38, 39] The BET surface area of the Glu@TNFs-3 (37.0 $m^2\ g^{-1}$) is approximately 30 times that of the etched TNFs (1.2 $m^2\ g^{-1}$), and is approximately 2 times higher than that of Saw@TNFs-3 (16.2 $m^2\ g^{-1}$).

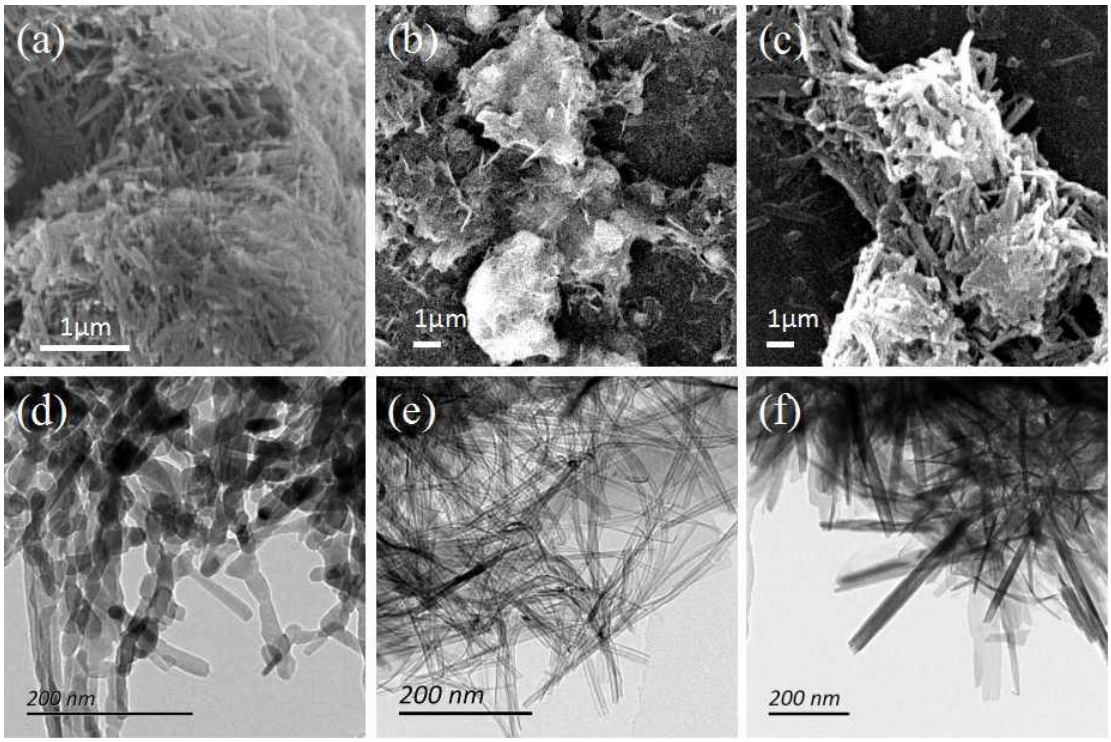

Fig. 2 SEM images of Glu@TNFs-3 **(a)**, Cel@TNFs-3 **(b)**, and Saw@TNFs-3 **(c)**; and TEM image of Glu@TNFs-3 **(d)** , Cel@TNFs-3 **(e)**, and Saw@TNFs-3 **(f)**. Synthetic conditions: 10 mol/L NaOH aqueous solution, 180°C, 48h

To investigate the morphological transformations, SEM and TEM images were collected. In detail, SEM images of Glu@TNFs-3 are displayed in **Fig. 2a**, the morphologies of Ti_3AlC_2 MAX phases are transformed from particles to nanofibers after etching. Compared with TNFs (**Fig. s2d**), Glu@TNFs-3 is fully wrapped by homogeneous hydrochar derived from glucose, and the surfaces possessed oxygen-containing functional groups.[40] SEM images of Cel@TNFs-3 are displayed in **Fig. 2b**, similarly, the morphologies are transformed from bulk particles (MAX phases) to nanofibers. Cel@TNFs-3 is coated by hydrochar derived from cellulose and big hydrocar particles formed at higher content of cellulose because of the hydrogen bond connections. SEM images of Saw@TNFs-3 are illustrated in **Fig. 2c**, the morphology is transformed from particles (MAX phases) to nanofibers. Sawdust was dissolved in NaOH solution and formed thick hydrochar layers. To confirm the structures between hydrochar and TNFs, TEM characterizations were performed and the TEM images are given in **Fig. 2d-f**. The hydrochar wrapped structures of Glu@TNFs-3 are successfully

constructed, the width of Glu@TNFs is between 10 nm and 50 nm, and the width of nanofibers is mainly concentrated around 20 nm. When cellulose was used, hydrochar-coated Ti_3AlC_2 nanofibers formed, having different diameters of 10 nm to 80 nm. As to Saw@TNFs, the diameters of nanofibers vary from 20 nm to 80 nm. All these results demonstrate that hydrochar-wrapped structures can be potentially optimized as to the char precursors and synthetic conditions.

Additionally, the chemical composition of these HCTNFs was evaluated by SEM-EDX elemental analysis (detailed results can be found in **Table S1, Section 3, ESI**). The NaOH etching removed Al elements and its content was lower than 4 at.% in the HCTNFs, but the Al content is 17 at.% in parent Ti_3AlC_2 phase.

Adsorption capacity studies

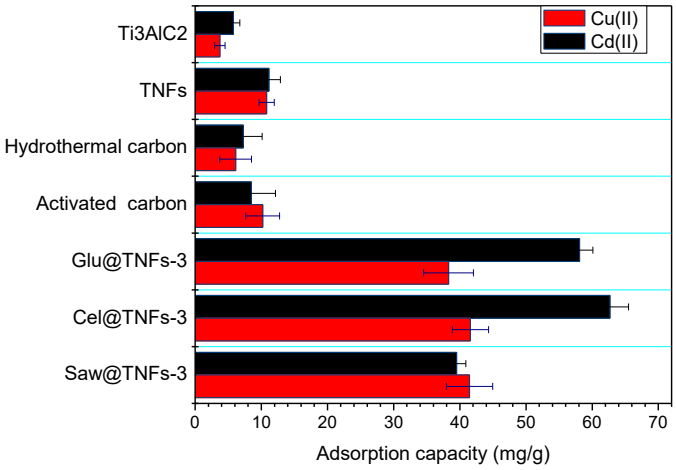

Fig. 3 Adsorption capacities of Ti_3AlC_2, TNFs, hydrothermal carbon, activated carbon and typical HCTNFs for Cu(II) and Cd(II). Conditions: pH(Cd) = 6, pH(Cu) = 5, $C(Cd)_{initial}$ = 100 mg L^{-1}, $C(Cu)_{initial}$ = 100 mg L^{-1}, m/V =1 g L^{-1} and T = 298 K.

The adsorption capacities of HCTNFs are displayed in **Section 5**, **ESI** and typical samples of Glu@TNFs-3, Cel@TNFs-3, and Saw@TNFs-3 were shown in **Fig. 3**. As to the adsorption of Cd(II), the HCTNFs exhibited much better adsorptive performances than those of Ti_3AlC_2, TNFs, Hydrothermal carbon and activated carbon, thus demonstrating that the distributed hydrochar on nanofibers outperform hydrochar big particles derived from glucose. The Glu@TNFs-2 and Cel@TNFs-3 showed similar adsorptive performances as Cd(II),

slightly better than Saw@TNFs-3 did. The change in precursor amount of glucose, cellulose, or sawdust added did not show an obvious improving trend of adsorptive performances. For Cu(II), it is obvious that more hydrochar precursors added resulted in higher the adsorption capacities of HCTNFs: Glu@TNFs was from 29.0 mg g^{-1} to 38.3 mg g^{-1}; Cel@TNFs was from 35.9 mg g^{-1} to 1.6 mg g^{-1}; Saw@TNFs was from 32.1 mg g^{-1} to 40.0 mg g^{-1}. Generally, the adsorption capacities of HCTNFs were much higher than those of Ti_3AlC_2, TNFs, Hydrothermal carbon and activated carbon, probably because of the abundant oxygen-containing functional groups on their surface and this will be discussed later on in the proposed mechanism.[41-43] Moreover, HCTNFs exhibited a higher adsorption capacity than many other materials reported in literature (detailed information was provided in **Table s2-s3** in **Section 6**, **ESI**).

Regeneration of adsorbents and sorption kinetics

To test the reusability of these adsorbents, the regeneration experiments were performed for 8 h by adding spent Glu@TNFs-3 in 30 ml of 0.2 mol L^{-1} HCl solution under stirring to remove Cd(II). After regeneration, the adsorption capacity of Glu@TNFs-3 was 61.1mg g^{-1}, which proved that Glu@TNFs-3 had strong reusability.

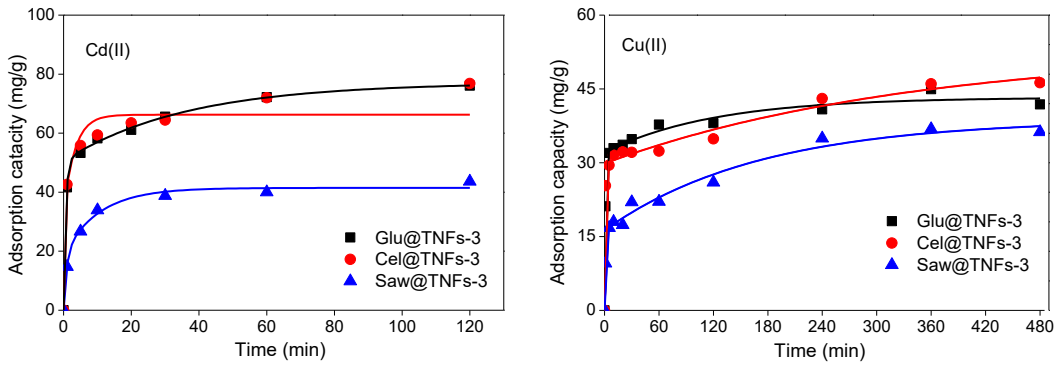

Fig. 4 Effect of contact time on the adsorption capacities of Glu@TNFs-3, Cel@TNFs-3, and Saw@TNFs-3 for Cd(II) **(Left)** and Cu(II) **(Right)**. Test conditions: pH(Cd) = 6, pH(Cu) = 5, $C(Cd)_{initial}$ = 100 mg L^{-1}, $C(Cu)_{initial}$ = 100 mg L^{-1}, m/V =1 g L^{-1} and T = 298 K.

Sorption kinetics were investigated to calculate the adsorption rate of Cd(II) and Cu(II) on Glu@TNFs-3, Cel@TNFs-3 and Saw@TNFs-3. **Fig. 4** shows the adsorption curves of

Cd(II) and Cu(II) on Glu@TNFs-3, Cel@TNFs-3, and Saw@TNFs-3 under different contact time periods. Results of sorption kinetics demonstrate that Cd(II) and Cu(II) uptake is a two distinct stage adsorption process. The rapid adsorption of Cd(II) and Cu(II) can be achieved within 10 min, and then a slow sorption stage is found for approaching equilibrium within 120 min for Cd(II) and 360 min for Cu(II). The rapid adsorption stage can be ascribed to abundant fresh functional groups on their surfaces, and then the surfaces are gradually occupied by Cd(II) or Cu(II) ions, which lead to a plodding adsorption stage.

The k_1 and q_e values of the pseudo-first-order model were obtained from the linear plot of $\ln(q_e - q_t)$ versus t (min) (figure not shown). Meanwhile, the plot of t/q versus t (min) was linearly fitted to calculate the pseudo-second-order correlation parameters (**Fig. s8a-f**, **Section 7**, **ESI**). According to the correlation coefficients (R^2) (given in **Table s4-s5**, **Section 7**, **ESI**) it can be concluded that the pseudo-second-order model fitted the kinetic data better than the pseudo-first-order model did. Moreover, the k_2 of Cu(II) adsorption on Saw@TNFs-3 was 6.5 × 10^{-3} g mg^{-1} min^{-1}, which was much higher than that on Glu@TNFs-3 and Cel@TNFs-3 (k_2 = 3.8 × 10^{-3} g mg^{-1} min^{-1}), indicating that the adsorption rate of Cu(II) on Saw@TNFs-3 was faster than that of Cu(II) on Glu@TNFs-3 and Cel@TNFs-3. The k_2 of Cd(II) adsorption on Glu@TNFs-3 was 4.2 × 10^{-3} g mg^{-1} min^{-1}, which was much higher than that on Cel@TNFs-3 (k_2 = 1.6 × 10^{-3} g mg^{-1} min^{-1}) and Saw@TNFs-3 (k_2 = 1.3 × 10^{-3} g mg^{-1} min^{-1}). This phenomenon further suggested that the rate-determining mechanism for Cd(II) and Cu(II) adsorption on Glu@TNFs-3, Cel@TNFs-3, and Saw@TNFs-3 was the chemisorption. Therefore, hydrochar-coated TNFs with more exposed surface functional adsorptive sites could adsorb these heavy metals faster than pure TNFs, Hydrothermal carbon, and activated carbon.

Mechanistic discussions

The experimental results of HCTNFs preparation demonstrated that hydrochar precursors of glucose, which completely dissolved in the synthetic solution, could form coherent and homogeneous hydro-wrapped structures due to the hydrogen-bonded interfacial materials between hydrochar and TNFs. On the contrary, cellulose and sawdust underwent hydrolysis first and then hydrogen-bonded with TNFs, this slow process gave rise to heterogeneously

distributed hydrochar particles over TNFs.

As to the adsorptive capacity, zeta potential and FT-IR analyses were used to seek for the underlying reasons. As a representative, the zeta potential of Glu@TNFs-3 was -10.9 mV at a pH=6, which can explain the efficient attraction of Cd(II) or Cu(II) owing to the electrostatic attraction as a driving force.[38] In addition, the numerous oxygen-containing functional groups are reported to be a main reason for heavy metal adsorption by HCTNFs,[44] and the supported hydrochar on TNFs exposed more adsorptive sites than Hydrothermal carbon, thereby performing better in the test adsorption of Cd(II) and Cu(II).

4. Conclusions

In conclusion, through the hydrothermal method, composite materials of "hydrochar-wrapped Ti_3AlC_2-derived nanofibers" (HCTNFs) were successfully prepared using glucose as the char precursor, and other precursors of cellulose and sawdust are also investigated. These products were examined in the removal of heavy metals from waste water, and the results demonstrated that the HCTNFs had a higher adsorption capacity than pure nanofiber of TNFs, hydrothermal carbon and commercial activated carbon particles. The reasons for the enhanced adsorption ability are believed to be the interfacial materials between hydrochar and TNFs which offer more surface functional groups and also exhibited strong interactions with heavy metals. Overall, we developed a scalable in-situ hydrothermal method to fabricate hydrochar-wrapped nanofibers that are derived from bulk Ti_3AlC_2 particles. The method is distinguishing because it is fluoride-free and controllable as to product morphology and adsorptive capacity, having the advantage of readily industrial applications.

Acknowledgement:

The authors thank the National Natural Science Foundation of China (NNSFC 21706134), the Young Natural Science Foundation of Jiangsu province (BK20170918) for financial support. Thank the technical support from the "Advanced analysis and testing center of Nanjing Forestry University".

References

1. W. J. Liu, H. Jiang and H. Q. Yu, *Chem Rev*, 2015, **115**, 12251-12285.

2. X. Zhang, K. Wilson and A. F. Lee, *Chem Rev*, 2016, **116**, 12328-12368.

3. H. S. Kambo and A. Dutta, *Renewable and Sustainable Energy Reviews*, 2015, **45**, 359-378.

4. J. Deng, M. Li and Y. Wang, *Green Chemistry*, 2016, **18**, 4824-4854.

5. J. Fang, L. Zhan, Y. S. Ok and B. Gao, *Journal of Industrial and Engineering Chemistry*, 2018, **57**, 15-21.

6. C. Santhosh, V. Velmurugan, G. Jacob, S. K. Jeong, A. N. Grace and A. Bhatnagar, *Chemical Engineering Journal*, 2016, **306**, 1116-1137.

7. J. Qiu, X.-F. Zhang, X. Zhang, Y. Feng, Y. Li, L. Yang, H. Lu and J. Yao, *Journal of Hazardous Materials*, 2018, **349**, 234-241.

8. J. Hu, S. Yang and X. Wang, *Journal of Chemical Technology & Biotechnology*, 2012, **87**, 673-681.

9. M. P. Waalkes, *Journal of inorganic biochemistry*, 2000, **79**, 241-244.

10. Y. Sun, S. Yang, Y. Chen, C. Ding, W. Cheng and X. Wang, *Environ Sci Technol*, 2015, **49**, 4255-4262.

11. G. Zou, J. Guo, Q. Peng, A. Zhou, Q. Zhang and B. Liu, *Journal of Materials Chemistry A*, 2016, **4**, 489-499.

12. C. Jiang, H. Chen, Y. Zhang, H. Feng, M. A. Shehzad, Y. Wang and T. Xu, *Chemical Engineering Journal*, 2018, **348**, 952-959.

13. I. Ciobanu, A. Josceanu, C. Guran and I. Minca, *Ion Chromatographic Method for Determination of Heavy Metals in Water*, 2015.

14. D. J. van Osch, D. Parmentier, C. H. Dietz, A. van den Bruinhorst, R. Tuinier and M. C. Kroon, *Chem Commun (Camb)*, 2016, **52**, 11987-11990.

15. H. Attia, D. J. Johnson, C. J. Wright and N. Hilal, *Desalination*, 2018, **439**, 31-45.

16. Z. Karim, S. Claudpierre, M. Grahn, K. Oksman and A. P. Mathew, *Journal of Membrane Science*, 2016, **514**, 418-428.

17. I. Akin, G. Arslan, A. Tor, Y. Cengeloglu and M. Ersoz, *Desalination*, 2011, **281**, 88-92.

18. C. Faur-Brasquet, K. Kadirvelu and P. Le Cloirec, *Carbon*, 2002, **40**, 2387-2392.

19. H. Wang, Y. Liu, J. Ifthikar, L. Shi, A. Khan, Z. Chen and Z. Chen, *Bioresource Technology*, 2018, **256**, 269-276.

20. M. Saber, F. Takahashi and K. Yoshikawa, *Environmental Science and Pollution Research*, 2018, **25**, 32721-32734.

21. Y.-J. Xu, G. Weinberg, X. Liu, O. Timpe, R. Schlögl and D. S. Su, *Advanced Functional Materials*, 2008, **18**, 3613-3619.

22. D. Mohan, A. Sarswat, Y. S. Ok and C. U. Pittman, *Bioresource Technology*, 2014, **160**, 191-202.

23. L. F. Chen, H. W. Liang, Y. Lu, C. H. Cui and S. H. Yu, *Langmuir*, 2011, **27**, 8998-9004.

24. J.-C. Lei, X. Zhang and Z. Zhou, *Frontiers of Physics*, 2015, **10**, 276-286.

25. W. G. Sloof, R. Pei, S. A. McDonald, J. L. Fife, L. Shen, L. Boatemaa, A.-S. Farle, K. Yan, X. Zhang, S. van der Zwaag, P. D. Lee and P. J. Withers, *Sci. Rep.*, 2016, **6**, 23040.

26. M. Ghidiu, M. R. Lukatskaya, M.-Q. Zhao, Y. Gogotsi and M. W. Barsoum, *Nature*, 2014, **516**, 78.

27. R. B. Rakhi, P. Nayak, C. Xia and H. N. Alshareef, *Scientific Reports*, 2016, **6**, 38465.

28. J. Cai, Y. He, X. Yu, S. W. Banks, Y. Yang, X. Zhang, Y. Yu, R. Liu and A. V. Bridgwater, *Renewable and Sustainable Energy Reviews*, 2017, **76**, 309-322.

29. X. Zhang, X. Ke, Z. Zheng, H. Liu and H. Zhu, *Applied Catalysis B: Environmental*, 2014, **150-151**, 330-337.

30. P. Asawaworarit, P. Daorattanachai, W. Laosiripojana, C. Sakdaronnarong, A. Shotipruk and N. Laosiripojana, *Chemical Engineering Journal*, 2019, **356**, 461-471.

31. S. Yuan, T. Li, Y. Wang, B. Cai, X. Wen, S. Shen, X. Peng and Y. Li, *Fuel*, 2019, **237**, 895-902.

32. S. Kajiyama, L. Szabova, K. Sodeyama, H. Iinuma, R. Morita, K. Gotoh, Y. Tateyama, M. Okubo and A. Yamada, *ACS Nano*, 2016, **10**, 3334-3341.

33. Q. Peng, J. Guo, Q. Zhang, J. Xiang, B. Liu, A. Zhou, R. Liu and Y. Tian, *J Am Chem Soc*, 2014, **136**, 4113-4116.

34. X. Xie, Y. Xue, L. Li, S. Chen, Y. Nie, W. Ding and Z. Wei, *Nanoscale*, 2014, **6**, 11035-11040.

35. M. Hara, T. Yoshida, A. Takagaki, T. Takata, J. N. Kondo, S. Hayashi and K. Domen, *Angew Chem Int Ed Engl*, 2004, **43**, 2955-2958.

36. M. Okamura, A. Takagaki, M. Toda, J. N. Kondo, K. Domen, T. Tatsumi, M. Hara and S. Hayashi, *Chemistry of Materials*, 2006, **18**, 3039-3045.

37. X. Zhang, L. J. Durndell, M. A. Isaacs, C. M. A. Parlett, A. F. Lee and K. Wilson, *ACS Catalysis*, 2016, **6**, 7409-7417.

38. P. Gu, J. Xing, T. Wen, R. Zhang, J. Wang, G. Zhao, T. Hayat, Y. Ai, Z. Lin and X. Wang, *Environmental Science: Nano*, 2018, **5**, 946-955.

39. Z. Sun, M. Li, L. Hu, X. Lu and Y. Zhou, *Journal of the American Ceramic Society*, 2009, **92**, 1695-1702.

40. A. K. Fard, G. McKay, R. Chamoun, T. Rhadfi, H. Preud'Homme and M. A. Atieh, *Chemical Engineering Journal*, 2017, **317**, 331-342.

41. A. B. Fuertes, M. C. Arbestain, M. Sevilla, J. A. Maciá-Agulló, S. Fiol, R. López, R. J. Smernik, W. P. Aitkenhead, F. Arce and F. Macías, *Soil Research*, 2010, **48**, 618-626.

42. Z. Liu, F.-S. Zhang and J. Wu, *Fuel*, 2010, **89**, 510-514.

43. S. E. Elaigwu, V. Rocher, G. Kyriakou and G. M. Greenway, *Journal of Industrial and Engineering Chemistry*, 2014, **20**, 3467-3473.

44. D. Kołodyńska, J. Krukowska and P. Thomas, *Chemical Engineering Journal*, 2017, **307**, 353-363.